Applied Catalysis B: Environmental 110 (2011) 148–153

Contents lists available at SciVerse ScienceDirect

Applied Catalysis B: Environmental

journal homepage: www.elsevier.com/locate/apcatb

Comparing Cr, and N only doping with (Cr, N)-codoping for enhancing visible light reactivity of TiO_2

Yuan Li[a,d,*], Wei Wang[a], Xiaofeng Qiu[b,1], Liang Song[a,2], Harry M. Meyer III[c], M. Parans Paranthaman[b], Gyula Eres[c], Zhenyu Zhang[c,d,3], Baohua Gu[a,**]

[a] Environmental Sciences Division, Oak Ridge National Laboratory, Oak Ridge, TN 37831, United States
[b] Chemical Sciences Division, Oak Ridge National Laboratory, Oak Ridge, TN 37831, United States
[c] Materials Science and Technology Division, Oak Ridge National Laboratory, Oak Ridge, TN 37831, United States
[d] Department of Physics and Astronomy, University of Tennessee, Knoxville, TN 37996, United States

ARTICLE INFO

Article history:
Received 20 June 2011
Received in revised form 12 August 2011
Accepted 26 August 2011
Available online 3 September 2011

Keywords:
Titania
Nanoclusters
Cation–anion codoping
Photodegradation
Solar energy

ABSTRACT

The photoreactivity of titania (TiO_2) nanoclusters with varying levels of N or Cr-doping, or (Cr, N)-codoping, was systematically investigated using photodegradation of methyl orange in aqueous suspensions. The shifting of the TiO_2 absorption edge into the visible spectral region that is primarily attributable to band gap narrowing was found to be a reliable metric for estimating the photoreactivity of the doped nanoclusters. Compared to the weak response with undoped and N-doped TiO_2, Cr-doping and (Cr, N)-codoping were found to significantly enhance photodegradation of methyl orange under visible light. The initial reaction rates increase from about 0 to above 1.6×10^{-2} min^{-1} when the doping concentration of Cr in TiO_2 increases from 0 to 5%. In stark contrast, under UV irradiation, doping is not only ineffective but also detrimental to the photoreactivity, and all doping including N or Cr only and (Cr, N)-codoping were found to reduce photoreactivity.

1. Introduction

Titanium oxide (TiO_2) is one of the most efficient and economical photocatalysts that has been studied extensively since 1970s for energy and environmental related applications, such as the degradation of organic contaminants in waste water and hydrogen generation from water splitting [1–7]. In recent years, the arising of renewable energy applications, especially solar technologies, has made the search and development of advanced materials that can effectively absorb and utilize solar light an emerging research field of great importance. However, one of the limitations of using TiO_2 as a photocatalyst is its large band gap energy (~3.2 eV for anatase and 3.0 eV for rutile), so that TiO_2 is only capable of absorbing ultraviolet light, which accounts a small portion of the solar spectrum [8].

To increase the photo-efficiency of TiO_2 under visible light, most research activities have been focused on ways to effectively narrow the band gap of TiO_2 by either cation or anion doping [4,6,9–29]. Here cation doping generally refers to the incorporation of transitional metal or rare-earth metal atoms into TiO_2 lattice, thereby introducing an impurity band below the conduction band level of TiO_2 and red-shifting the band gap of TiO_2 into visible regime [9–14]. For example, in a study of the sol–gel synthesis of TiO_2 nanoparticles doped with different metal ions at various doping levels, Choi et al. [9] found that Pt and Cr doped TiO_2 have the best photocatalytic activities. However, a major drawback of the cation doping scheme lies in the fact that most metal ions only have limited thermodynamic solubility in TiO_2 lattice. As a result, excess surface dopants can act as electron–hole recombination centers [15]. Alternatively, substitutional doping of anions such as N, C, B into the O sites in TiO_2 was found to be effective in reducing the band gap of TiO_2 by mixing the 2*p* states of dopants with O 2*p* state [4,6,16–21,24–26,29]. For instance, using sputtering technique, Asahi et al. [4] reported that the doping of TiO_2 films with N is promising in enhancing visible light photoreactivity. However, despite these reported successes, the characteristics of N electronic states in the TiO_2 lattice are still under debate [15,26].

Using first principles calculations and in an attempt to further increase both the thermodynamic and kinetic solubilities of

* Corresponding author at: Environmental Sciences Division, Oak Ridge National Laboratory, P.O. Box 2008, Oak Ridge, TN 37831, United States. Tel.: +1 865 241 1206; fax: +1 865 576 8543.
** Corresponding author at: Environmental Sciences Division, Oak Ridge National Laboratory, P.O. Box 2008, Oak Ridge, TN 37831, United States. Tel.: +1 865 574 7286; fax: +1 865 576 8543.
E-mail addresses: liy1@ornl.gov (Y. Li), gub1@ornl.gov (B. Gu).
[1] Present address: IBM T.J. Watson Research Center, P.O. Box 218, Route 134, Yorktown Heights, NY10598, United States.
[2] Present address: College of Chemistry and Chemical Engineering, Ocean University of China, Qingdao 266100, PR China.
[3] Present address: ICQD/HFNL, University of Science and Technology of China, Hefei 230026, PR China.

0926-3373/$ – see front matter © 2011 Elsevier B.V. All rights reserved.
doi:10.1016/j.apcatb.2011.08.037

dopants in TiO_2, Zhu et al. [15] recently proposed a new doping scheme, namely the non-compensated *n–p* codoping. In this doping scheme, the Columbic attraction between the *n–p* codoped pair enhances the incorporation of both dopants into TiO_2 lattice, and the non-compensated nature of dopants can ensure the creation of intermediate bands in the gap region of TiO_2, effectively narrowing its band gap [15]. Non-compensated codopant pair of Cr and N was predicted to have optimal photoactivity [15]. By trial-and-error, several previous studies have examined the effects of codoping on improving the photocatalytic activities of TiO_2 [30–33], although results to date are inconclusive. For example, using a combination of sol–gel synthesis and thermal annealing under ammonia, Pan and Wu [31] studied the effect of Cr and N codoping on the photodegradation of methylene blue and isopropyl alcohol under visible light. They observed that the codoped TiO_2 was in fact less reactive than either Cr or N singly doped TiO_2 [31].

In this report, we use a modified sol–gel synthesis technique and systematically investigate and compare photocatalytic reactivities of a range of (Cr, N)-codoped and Cr or N singly doped TiO_2 at varying dopant concentrations and under either UV or visible light irradiation. We show that both Cr doping and (Cr, N)-codoping effectively shift the TiO_2 absorption edge into the visible spectral region, leading to greatly enhanced visible light photoreactivity. However, the (Cr, N)-codoping did not show improved photoreactivity as compared with Cr singly doped TiO_2 under visible light. All doped and codoped TiO_2 were also found to be detrimental to the photoreactivity under UV irradiation.

2. Experimental

2.1. Synthesis of doped TiO_2 nanoparticles

A modified sol–gel hydrolysis method was utilized to synthesize nanocrystalline Cr or N singly doped and (Cr, N) codoped TiO_2 particles [15]. Tetrakis(diethyamino) titanium ($Ti(N(C_2H_5)_2)_4$) and chromium nitrate ($Cr(NO_3)_3{\cdot}9H_2O$) were used as the sources of N and Cr dopants, respectively, and titanium isopropoxide ($Ti(OCH(CH_3)_2)_4$) was used as the precursor for TiO_2.

For the synthesis of (Cr, N)-codoped TiO_2, we first added an appropriate amount of $Cr(NO_3)_3{\cdot}9H_2O$, calculated based on the desired Cr dopant concentration in the range from 0.4 to 5 at.%, into a mixture of 20 mL ethanol and 20 mL deionized water and stirred for at least 3 h. Second, a precursor solution was prepared by adding a given amount of $Ti(N(C_2H_5)_2)_4$ into 20 mL ethanol and immediately followed by adding 2 mL of $Ti(OCH(CH_3)_2)_4$. Third, the precursor solution was added dropwise to the $Cr(NO_3)_3{\cdot}9H_2O$ containing mixture under vigorous stirring. The reaction mixture was allowed to react overnight and the resulting gel precipitate was centrifuged, washed five times with ethanol, and dried at 110 °C for 12 h. Finally, the amorphous TiO_2 was calcinated at 550 °C in air for 3 h to obtain nanocrystalline powder. For the preparation of undoped TiO_2 and Cr or N singly doped TiO_2, the same procedure was adopted except that no Cr or N dopants were added to synthesize TiO_2, or only Cr or N dopant was added for the synthesis of singly doped Cr–TiO_2 or N–TiO_2.

The as-synthesized TiO_2, N–TiO_2, Cr–TiO_2 and (Cr, N)–TiO_2 samples are designated as T, NT, CrT and CrNT respectively, followed by numbers in parentheses indicating the nominal atomic percentages of dopants. For instance, NT(5) represents N doping at 5% N; CrT(5) represents Cr doping at 5%; CrNT(5, 5) represents Cr and N-codoping at 5% each. The calculated starting compositions for as-synthesized Cr–TiO_2 samples were 0.4, 0.6, 1.2, 1.8, 3 and 5% Cr. For the N–TiO_2, they were 1, 2 and 5% N. The starting atomic percentages for (Cr, N)–TiO_2 were (0.4, 2), (0.6, 2), (1.2, 2), (1.8, 2), (3, 3) and (5, 5).

2.2. Characterization of the doped TiO_2 nanoparticles

The crystalline structure of as-synthesized TiO_2 samples was examined by Raman spectroscopy using a Renishaw micro-Raman system equipped with a 785 nm near-infrared diode laser and by X-ray diffraction (XRD) using a Scintag DMC 008 X-ray diffractometer with Cu Kα radiation. Raman and XRD spectra of standard anatase and rutile powder (purchased from Sigma–Aldrich) were also collected as references. Morphological information of TiO_2 nanoparticles was evaluated by a Hitachi HD2000 scanning transmission electron microscope (STEM) system equipped with energy-dispersive X-ray (EDX) spectroscopy. The UV–vis reflectance spectra were recorded with a Photonics 400 Series UV–vis spectrophotometer in the range of 350–950 nm. X-ray photoelectron spectroscopy (XPS) measurements were performed on a K-Alpha Thermo-Fischer Scientific XPS system equipped with Al Kα radiation. Selected XPS spectra were given in the Supplementary Data, Section 1.

2.3. Photoreactivity measurements

Photoreactivity of as-synthesized TiO_2 was evaluated by measuring photodegradation rates of methyl orange (MO). While it is recognized that the use of such dyes has its limitations due to surface sensitization, MO has been widely used to assess the performance of photocatalytic materials due to its sensitivity and simplicity of use [13,34–38]. The experiment was performed under either UV or visible light irradiation. A 100 W, 365 nm mercury lamp (UVP, LLC) was utilized as the UV-A (315–400 nm) light source (relevant to natural sunlight irradiation). Visible light was generated by passing the incident beam from a 450 W Xe Arc lamp (Newport Corp.) first through an 8 cm × 8 cm × 8 cm glass bottle filled with deionized water and then through an Andover optical filter with a cutoff wavelength at 420 nm. The rate of MO degradation was quantified by changes in absorbance at 664 nm using a HP 8453 UV–vis spectrophotometer. To ensure a linear absorbance-concentration response, the initial concentration of MO was controlled so that the measured absorbance at 664 nm by a 1 cm path length cuvette is about 1 (corresponding to the MO concentration of ~14 mg/L or 43 μM). The nanoparticles were first dispersed in MO solution at 1 g/L and allowed to react in dark for an hour to reach equilibrium so that potential sorption and chemical degradation of MO can be accounted for. Time-sequenced sample aliquots were then collected from the reaction mixture and analyzed following UV or visible light exposure. Two or three runs were repeated for each data set, and each data point represents an average with an estimated experimental error being ±3%. In addition to as-synthesized samples, Aeroxide® TiO_2 P25 catalyst (Evonik Degussa Corp.) was used as a reference material and examined under the same conditions. Blank controls where MO solution was irradiated by UV or visible light in the absence of TiO_2 nanoparticles were also assessed, and results showed negligible degradation of MO over time.

3. Results

3.1. Characteristics of doped TiO_2 nanoclusters

The representative Raman spectra of as-synthesized TiO_2 nanoclusters as well as reference anatase and rutile samples are shown in Fig. 1a. Anatase was identified as the major crystalline phase in all synthesized samples. Only two samples with the highest amount of Cr doping, CrT(5) and CrNT(5,5), showed a small Raman

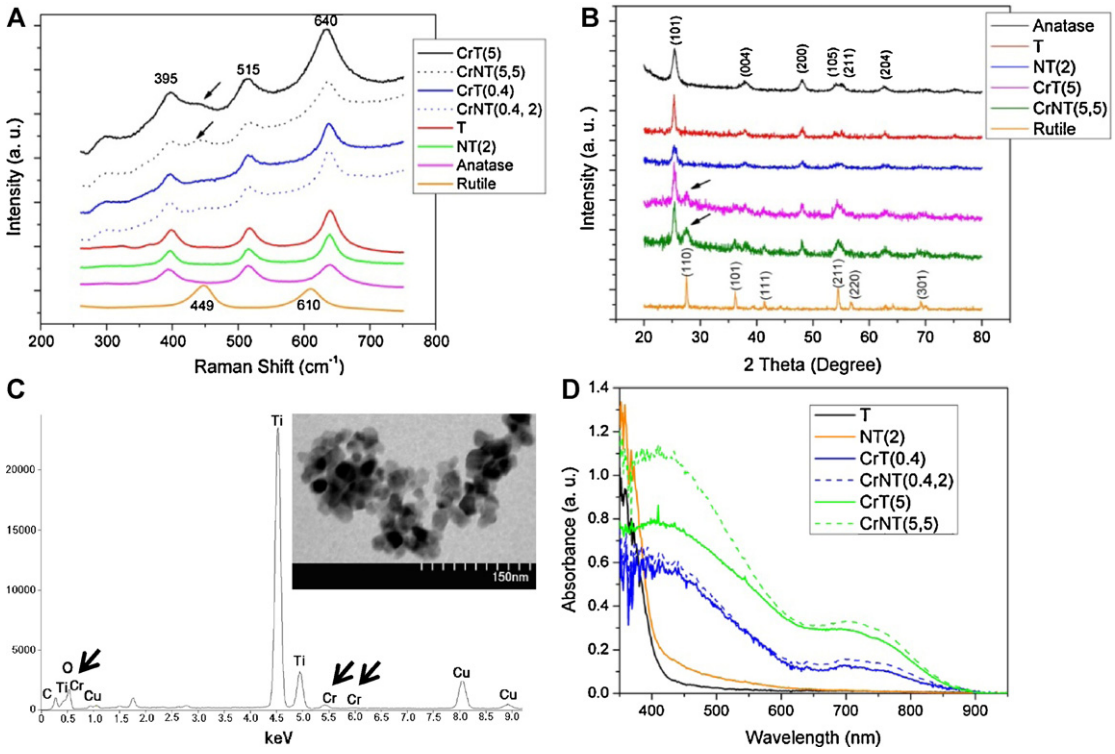

Fig. 1. Characterization of as-synthesized TiO_2, singly doped N–TiO_2 and Cr–TiO_2, and codoped (Cr, N)–TiO_2 nanoparticles: (A) micro-Raman spectra; (B) XRD spectra; (C) EDX analysis and a STEM image of a representative Cr–TiO_2 sample with nominal Cr doping level at 1.8%; (D) UV–vis reflectance spectra. Arrows in (a) and (b) indicate the presence of rutile phase, and those in (c) show the position of Cr peaks.

shift at about 446 cm^{-1} (marked by arrows), which is assigned to the rutile phase. No Raman bands corresponding to Cr–O or Ti–N vibrational modes were identified, likely because of relatively low dopant concentrations. Similarly, XRD measurements (Fig. 1b) showed that Cr-doped or codoped samples mostly exist in the anatase form. Rutile phase is not found in the pure TiO_2 and N–TiO_2 samples, but is in the 5% Cr doped and (Cr, N) codoped samples as confirmed by X-ray diffraction at $2\theta = 27.5^\circ$ for samples CrT(5) and CrNT(5,5). These observations indicate that Cr doping lowers the anatase-rutile phase transition temperature of TiO_2 [9,14].

The morphology of as-synthesized TiO_2 nanoclusters was characterized by STEM and EDX spectroscopy, and Fig. 1c represents one of the Cr-doped TiO_2 samples. Nanocrystalline TiO_2 with sizes typically about 15–20 nm was observed, and EDX analysis confirmed the presence of Cr (marked by arrows in Fig. 1c). As expected, the observed peak intensity for Cr relative to that for Ti increased as the Cr dopant concentration increased for both Cr–TiO_2 and (Cr, N)–TiO_2 (Supplementary Data, Section 2).

UV–vis reflectance spectral measurements were used to determine the TiO_2 absorption edge shift, which is indicative of bandgap narrowing through doping or codoping (Fig. 1d). The spectrum of undoped TiO_2 shows a sharp absorption edge at about 415 nm, and doping with N alone had a negligible effect on shifting the absorption edge. On the other hand, Cr doped and (Cr, N)-codoped samples showed extended absorption spectra into the visible region, with an absorption shoulder centered around 700 nm. This absorption edge shift can be explained by the *d–d* transition, $^4A_2 \rightarrow {}^4T_2$, of Cr^{3+} ions in octahedral structures [14,30]. As the Cr dopant concentration increased from 0.4% to 5%, the absorption also increased. In addition, (Cr, N)-codoped TiO_2 showed slightly higher photo-absorbance than singly doped Cr–TiO_2 at the same Cr dopant concentration.

3.2. Visible light reactivity

The photoreactivity of as-synthesized Cr–TiO_2, N–TiO_2, and (Cr, N)–TiO_2 nanoparticles was subsequently examined under visible light irradiation (at 420 nm and above). Fig. 2a and b compare the degradation of MO as a function of irradiation time in the presence of Cr doped or (Cr, N) codoped TiO_2 at varying Cr-doping levels. The pure TiO_2 and singly doped N–TiO_2 had negligible visible light activities, similar to the commercial P25 catalyst. On the other hand, as the Cr doping level increased, Cr–TiO_2 and (Cr, N)–TiO_2 samples showed increasing photodegradation rates of MO, both demonstrating the potential as visible-light active photocatalysts.

For quantitative analysis, the pseudo first-order reaction kinetics was used to fit the MO degradation data within the first 90 min of light irradiation (Fig. 2). Table 1 lists the initial reaction rate constants as well as total percentages of MO degradation after 3 h of reaction. Results indicate that, for both Cr-doped and (Cr, N)-codoped TiO_2, the reaction rates increased with increasing Cr doping levels. However, at the same Cr doping level (between 0% and 1.8%), the codoped (Cr, N)–TiO_2 samples showed slightly lower reaction rates and lower percentages of MO degradation than the corresponding singly doped Cr–TiO_2 samples. This observation agrees with those reported by Pan and Wu [31], who found that (Cr, N)-codoping had no beneficial effects in degrading methylene blue and isopropyl alcohol under visible-light (>460 nm). However, when the Cr doping concentration increased from 3% to 5%, the reaction rates and total percentages of MO degradation become comparable for both Cr-doped TiO_2 and (Cr, N)-codoped TiO_2 (Fig. 2). Following the initial 90 min of reaction, the rates became slower as demonstrated by the leveling off of the degradation curve (Fig. 2). This apparent two-stage reaction kinetics has been observed previously, for example, in the degradation of MO over iron (Fe)-doped TiO_2 [13], and is thought to result from possible

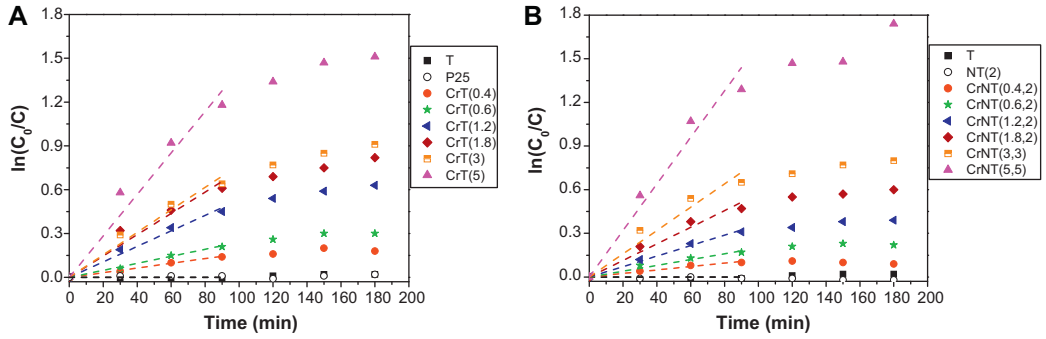

Fig. 2. Initial first-order fitting of the $\ln(C_0/C)$ versus time for the photodegradation of methyl orange under visible light by: (A) as-synthesized TiO_2 or Cr-doped TiO_2 and a commercial Aeroxide® TiO_2 (P25) catalyst and (B) TiO_2, N-doped TiO_2, and (Cr, N)-codoped TiO_2. Dashed lines are the linear fit of the initial reaction (≤90 min). Each data point represents an average of 2 to 3 runs with an estimated experimental error of ±3%.

chemical adsorption of peroxide during photocatalysis on the surface of TiO_2 [39].

3.3. UV light reactivity

The photodegradation of MO by N–TiO_2, Cr–TiO_2 and (Cr, N)–TiO_2 nanoparticles was further examined under UV irradiation (at 365 nm) to better understand how N, Cr doping and codoping may affect the photocatalytic properties of TiO_2. Fig. 3a shows that, under the same experimental conditions, P25 and as-synthesized pure TiO_2 degraded almost 100% MO after 35 and 75 min of UV irradiation (as demonstrated by $\ln(C_0/C) > 4$). The N-doping alone was found to reduce the photoreactivity of TiO_2, and the degradation rate decreased from about 3.3×10^{-2} to 1.3×10^{-3} min^{-1} as N dopant concentration increased from 0% to 5% (Table 1). However, as opposed to those observed for Cr–TiO_2 and (Cr, N)–TiO_2 under visible light (Fig. 2), the degradation curves of MO by TiO_2 and N–TiO_2 concaved up (Fig. 3a), indicating faster decays during the latter stage of the reactions. This same phenomenon was reported previously for undoped TiO_2 under UV light [13]. It was hypothesized that undoped TiO_2 has higher quantum efficiency than doped TiO_2 under UV light and subsequently the accumulation of peroxide on the surface of undoped TiO_2 is limited [13], leading to increased reaction rates.

Fig. 3b and c summarizes the results of MO degradation under UV irradiation by Cr–TiO_2 and (Cr, N)–TiO_2 at varying Cr-doping levels. Similar to those observed for N-doped TiO_2 (Fig. 3a), Cr–TiO_2 and (Cr, N)–TiO_2 showed a much lower reactivity than the undoped TiO_2, suggesting that Cr-doping and (Cr, N)-codoping are also detrimental to photocatalytic reactivities of TiO_2 under UV light. As Cr doping level increased from 0.4% to 5%, the initial reaction rates increased from 6×10^{-3} to 1.2×10^{-2} min^{-1} for Cr-doped TiO_2 and from 1.8×10^{-3} to 1.9×10^{-2} min^{-1} for (Cr, N)-codoped TiO_2, respectively, consistent with the observations under visible light irradiation. The reaction rates and amounts of MO degraded for Cr–TiO_2 are generally comparable to those of (Cr, N)–TiO_2, except for Cr–TiO_2 at 0.4%. The MO degradation rate by Cr–TiO_2 at 0.4% increased (concaved up) during the latter stage of the reaction, similar to that observed for the pure TiO_2 or N-doped TiO_2 (Fig. 3a). This fast decay rate following 90 min UV exposure resulted in a significantly higher amount of MO degradation in 3 h than the rest of the Cr-doped TiO_2 samples.

4. Discussion

4.1. Influences of dopants on visible light reactivity of TiO_2

The photocatalytic reaction generally involves four processes including charge carrier generation, trapping, recombination and

Table 1
Photocatalytic reactivity of Cr and N-doped or codoped TiO_2 for the degradation of methylene orange (MO) under either UV or visible light irradiation.

TiO_2 nanoparticle	Initial first order reaction rate constant ($\times 10^{-3}$ min^{-1})		Total MO degraded (%) in 3 h[b]	
	Visible light	UV light	Visible light	UV light
P25	0	72 ± 2	ND[c]	100%
As-synthesized TiO_2	0	33 ± 1	ND	100%
Cr–TiO_2 (0.4%)	1.6 ± 0.1	6.0 ± 0.1	17%	85%
Cr–TiO_2 (0.6%)	2.4 ± 0.7	–	26%	–
Cr–TiO_2 (1.2%)	5.2 ± 0.2	–	47%	–
Cr–TiO_2 (1.8%)	7.3 ± 0.6	8.0 ± 0.7	56%	59%
Cr–TiO_2 (3%)	7.7 ± 0.5	9.0 ± 0.5	60%	65%
Cr–TiO_2 (5%)	14 ± 1	12 ± 0.4	78%	70%
N–TiO_2 (1%)	–[a]	6.2 ± 0.2	–	84%
N–TiO_2 (2%)	0	2.6 ± 0.1	ND	44%
N–TiO_2 (5%)	–	1.3 ± 0.1	–	35%
(Cr, N)–TiO_2 (0.4%, 2%)	1.2 ± 0.1	1.8 ± 0.2	8%	16%
(Cr, N)–TiO_2 (0.6%, 2%)	2.0 ± 0.1	–	20%	–
(Cr, N)–TiO_2 (1.2%, 2%)	3.6 ± 0.1	–	32%	–
(Cr, N)–TiO_2 (1.8%, 2%)	5.7 ± 0.4	6.1 ± 0.3	45%	52%
(Cr, N)–TiO_2 (3%, 3%)	8.0 ± 0.6	10 ± 1	55%	61%
(Cr, N)–TiO_2 (5%, 5%)	16 ± 1	19 ± 2	82%	84%

[a] "–" indicates that experimental data not available.
[b] Estimated experimental error is ±3%.
[c] ND = the degradation of MO not detected.

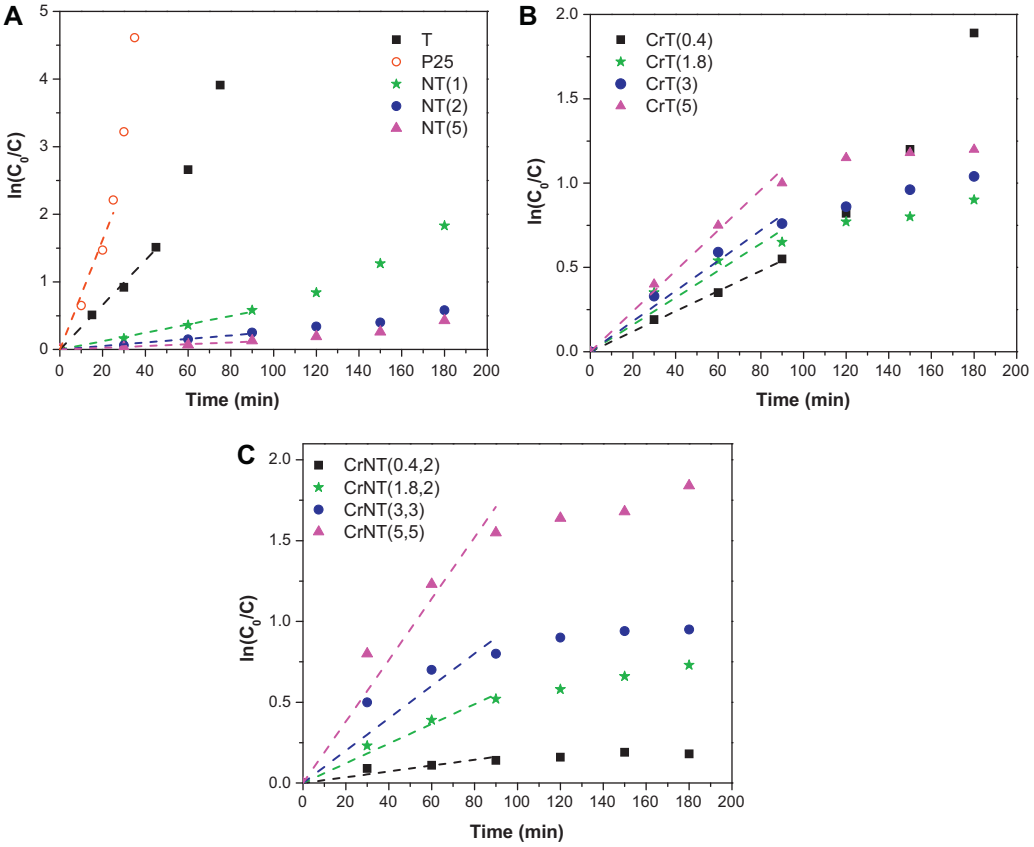

Fig. 3. Initial first-order fitting of the $\ln(C_0/C)$ versus time for the photodegradation of methyl orange under UV light by: (A) as-synthesized TiO_2 or N-doped TiO_2 and a commercial Aeroxide® TiO_2 (P25) catalyst, (B) Cr-doped TiO_2, and (C) (Cr, N)-codoped TiO_2. Dashed lines are the linear fit of the initial reaction (≤90 min). Each data point represents an average of 2 to 3 runs with an estimated experimental error of ±3%.

interfacial charge transfer. To examine how dopants such as Cr and N affect the photocatalytic efficiency of TiO_2, the influences of doping on charge carrier generation and recombination are often considered. When a photon is absorbed by TiO_2, an electron–hole pair, also known as charge carrier, is generated. Since the as-synthesized TiO_2 has a sharp absorption edge at about 415 nm, TiO_2 alone did not possess much visible light reactivity. Doping TiO_2 with N alone also showed little improvement in band gap narrowing (Fig. 1d) and therefore negligible visible light photoreactivity (Fig. 2). On the other hand, both Cr doping and (Cr, N) codoping significantly extended the absorption of TiO_2 into visible light regime and thus led to enhanced visible light reactivity. Furthermore, as Cr doping level increased, the observed visible light absorbance for both Cr–TiO_2 and (Cr, N)–TiO_2 increased (Fig. 1d), so as the photodegradation rates of MO.

The number of recombination sites is particularly important in determining the reactivity of photocatalysts [40]. Photo-generated electrons and holes can recombine at impurity sites, resulting in the annihilation of an electron–hole pair and thus a net loss of photo-efficiency. This is well illustrated by the fact that, although rutile has lower band gap that extends into visible light region than anatase, anatase usually shows higher photoreactivity than rutile because anatase has a much lower charge carrier recombination rate [40]. Wilke and Breuer [12] used the time-resolved photo-charge (TRPC) measurements to examine the lifetime of photon-generated charge carriers and found that Cr^{3+} doping greatly reduces electron–hole lifetime under UV–vis light. This reduction is the most significant when Cr^{3+} doping is less than 1% but levels off with increasing Cr concentrations from 1% to 3.5%. Therefore, Cr doping seems to increase the rate of recombination and results in a negative effect on the overall photoreactivity of TiO_2. Similarly, N dopants may act as charge carrier recombination centers based on observations that, when N dopant concentration increased from 1% to 5%, the rate of MO degradation under UV irradiation decreased nearly 5 times (Fig. 3a, Table 1). Pan and Wu [31] suggested that the presence of extra imperfection in (Cr, N)-codoped TiO_2 lattice is likely responsible for decreased photoreactivity when compared with that of Cr-singly doped TiO_2.

We therefore conclude that, as Cr doping or (Cr, N) codoping level increases, the effect of the enhanced visible light absorption (or charge carrier generation) outweighs the negative influences from increasing numbers of charge carrier recombination centers. As a result, visible light photoreactivity of Cr–TiO_2 and (Cr, N)–TiO_2 both increase as Cr doping levels increase. We note that, at Cr doping concentrations above 5%, excess Cr appeared to exist on the surfaces of doped TiO_2 (Supplementary Data, Section 1), leading to an apparently much higher percentage of MO degradation than those at relatively low Cr-doping levels (Table 1). As a result, we did not attempt to further increase Cr doping concentrations above 5%, partly due to potential concerns on Cr toxicity. Alternative approaches such as *n–p* codoping using pulse laser deposition may be explored in future studies in order to increase both the thermodynamic and kinetic solubilities [15] so as to observe an optimal Cr doping level for enhancing visible light photoreactivity.

4.2. *Influences of dopants on UV light reactivity of TiO_2*

Under UV irradiation, both Cr- and N-doping are detrimental to the photodegradation of MO because both dopants acted as electron–hole recombination centers. Doping with only 0.4% Cr in Cr-doped and (Cr, N)-codoped TiO_2 resulted in dramatic decrease in the initial photodegradation rate of MO. However, further increase

in Cr doping levels from 0.4% to 5% slightly benefited the UV-light reactivity or photodegradation of MO by both Cr-doped or (Cr, N)-codoped TiO_2 (Table 1), probably due to slightly improved UV absorption by comparing the absorbances between CrT(5) and CrT(0.4), and between CrNT(5) and CrNT(0.4) at 365 nm (Fig. 1d). Therefore, the overall UV light reactivity of both Cr–TiO_2 and (Cr, N)–TiO_2 first decreased and then increased with increasing Cr doping levels from 0% to 5%, similarly to those observed by Wilke and Breuer [12].

4.3. Photoreactivity comparisons between Cr-doped and (Cr, N)-codoped TiO_2

In this study, (Cr, N)-codoping was successful in enhancing visible light absorption but did not show significantly enhanced photoreactivity when compared with Cr singly doped TiO_2 at the same Cr-doping levels. We speculate that a major competing effect here is that the extra N dopants in (Cr, N)–TiO_2 may have led to more electron–hole recombination centers than those in Cr-doped TiO_2 (Fig. 3).

Our observations agree in part with theoretical predictions that non-compensated (Cr, N) codoping enhances visible light absorption of TiO_2 [15] but this enhanced photoabsorption did not result in enhanced photoreactivity of TiO_2. We point out two possible explanations that may contribute to this discrepancy. First, the concept of non-compensated cation–anion codoping is based on idealized chemical structures that Cr and N dopants are incorporated simultaneously into the substitutional lattice structure of TiO_2. Using the current sol–gel method, Cr and N dopants are introduced stepwise, not simultaneously as a dopant pair, so that N and Cr are most likely doped in interstitial sites [15]. Although different synthesis schemes such as sputtering in N_2/Ar gas [4], annealing under NH_3 atmosphere [31], anodizing in ammonium fluoride [6], and adding non-precursor chemicals that contain N [16,32] may result in somewhat different characteristics of doped or codoped nanomateirals, none of these techniques are capable of producing codoped TiO_2 with Cr and N truly as a substitutional dopant pair. Efforts aimed at using alternative techniques to synthesize codoped TiO_2 photocatalysts such as single or dual target pulsed laser deposition may hold promise to better validate theoretical predictions. Second, in comparison with the single cation or anion doping scheme, the two most significant advantages of non-compensated cation–anion codoping are increased dopant solubility and narrowed band gap [15]. However, many other factors, such as the number of charge carrier recombination sites, the crystalline phase and composition of codoped nanomaterials, also strongly influence the overall photocatalytic reactivity.

5. Conclusions

We compare the photoreactivty of Cr, and N only doped TiO_2 nanoclusters with that of (Cr, N)-codoped nanoclusters. The optical absorption spectra show that N doping fails to significantly red-shift the band edge of TiO_2. In contrast, both Cr doping and (Cr, N)-codoping result in optical absorption strongly red shifted into the visible spectral region that is attributed to band gap narrowing of TiO_2. The photodegradation of MO in aqueous suspensions used for probing the photoreactivity indicates that N-doping has a weak effect while Cr-doping and (Cr, N)-codoping produce strong photoreactivity in the visible light region. The visible light reactivity of both Cr–TiO_2 and (Cr, N)–TiO_2 increases with increasing Cr doping levels. In contrast, under UV irradiation, all doped TiO_2 shows lower photoreactivity than undoped TiO_2 likely caused by the dominating role of Cr and N dopants as charge carrier recombination centers. Future studies are needed on utilizing alternative synthetic approaches that can produce truly substitutionally doped TiO_2 to fully realize the benefit of *n*–*p* codoping in enhancing visible-light photoreactivity of TiO_2 for energy applications.

Acknowledgements

This work was sponsored in part by the US Department of Energy (DOE) Office of Basic Energy Sciences, Materials Science and Engineering Division, and Laboratory Directed Research and Development (LDRD) Program of Oak Ridge National Laboratory (ORNL), which is managed by UT-Battelle LLC for the U.S. DOE under contract No. DE-AC05-00OR22725. STEM measurement was conducted at ORNL Center for Nanophase Materials Sciences, which is sponsored by the Scientific User Facilities Division of DOE.

Appendix A. Supplementary data

Supplementary data associated with this article can be found, in the online version, at doi:10.1016/j.apcatb.2011.08.037.

References

[1] A. Fujishima, K. Honda, Nature 238 (1972) 37–38.
[2] M.A. Fox, M.T. Dulay, Chem. Rev. 93 (1993) 341–357.
[3] M.R. Hoffmann, S.T. Martin, W. Choi, D.W. Bahnemann, Chem. Rev. 95 (1995) 69–96.
[4] R. Asahi, T. Morikawa, T. Ohwaki, K. Aoki, T. Taga, Science 293 (2001) 269–271.
[5] X. Hu, G. Li, J.C. Yu, Langmuir 26 (2010) 3031–3039.
[6] O.K. Varghese, M. Paulose, T.J. LaTempa, C.A. Grimes, Nano. Lett. 9 (2009) 731–737.
[7] A. Li, B.C. Sun, N. Fahruddin, J.X. Zhao, D.T. Pierce, Synthesis and Analysis Applications of TiO_2-Based Nanomaterials, Wiley-VCH Verlag GmbH & Co. KGaA, 2010.
[8] M. Gratzel, Nature 414 (2001) 338–344.
[9] J. Choi, H. Park, M.R. Hoffmann, J. Phys. Chem. C 114 (2010) 783–792.
[10] E. Borgarello, J. Kiwi, M. Gratzel, E. Pelizzetti, M. Visca, J. Am. Chem. Soc. 104 (1982) 2996–3002.
[11] Z. Zhang, C.-C. Wang, R. Zakaria, J.Y. Ying, J. Phys. Chem. B 102 (1998) 10871–10878.
[12] K. Wilke, H.D. Breuer, J. Photochem. Photobiol. A: Chem. 121 (1999) 49–53.
[13] X.H. Wang, J.-G. Li, H. Kamiyama, Y. Moriyoshi, T. Ishihaki, J. Phys. Chem. B 110 (2006) 6804–6809.
[14] C.-C. Tsai, H. Teng, Appl. Surf. Sci. 254 (2008) 4912–4918.
[15] W. Zhu, X. Qiu, V. Iancu, X.-Q. Chen, H. Pan, W. Wang, N.M. Dimitrijevic, T. Rajh, H.M. Meyer III, M.P. Paranthaman, G.M. Stocks, H.H. Weitering, B. Gu, G. Eres, Z. Zhang, Phys. Rev. Lett. 103 (2009) 226401.
[16] X. Qiu, Y. Zhao, C. Burda, Adv. Mater. 19 (2007) 3995–3999.
[17] C. Burda, Y. Lou, X. Chen, A.C.S. Samia, J. Stout, J.L. Gole, Nano. Lett. 3 (2003) 1049–1051.
[18] T. Ohno, M. Akiyoshi, T. Umebayashi, K. Asai, T. Mitsui, M. Matsumura, Appl. Catal. A 265 (2004) 115–121.
[19] E.A. Reyes-Garcia, Y. Sun, K.R. Reyes-Gil, D. Raftery, Solid State Nucl. Magn. Reson. 35 (2009) 74–81.
[20] P. Zabek, J. Eberl, H. Kisch, Photochem. Photobiol. Sci. 8 (2009) 264–269.
[21] Y. Izumi, T. Itoi, S. Peng, J. Phys. Chem. C 113 (2009) 6706–6718.
[22] E. Gyorgy, A.P. Pino, P. Serra, J.L. Morenza, Surf. Coat. Technol. 173 (2003) 265–270.
[23] D. Li, H. Haneda, S. Hishata, N. Ohashi, Chem. Mater. 17 (2005) 2588–2595.
[24] Y. Huang, W. Ho, S. Lee, L. Zhang, G. Li, J.C. Yu, Langmuir 24 (2008) 3510–3516.
[25] J.C. Yu, J. Yu, W. Ho, Z. Jiang, L. Zhang, Chem. Mater. 14 (2002) 3808–3816.
[26] X. Chen, C. Burda, J. Am. Chem. Soc. 130 (2008) 5018–5019.
[27] L. Palmisano, V. Auguliaro, A. Sclafani, M. Schiavello, J. Phys. Chem. 92 (1988) 6710–6713.
[28] C. Martin, I. Martin, V. Rives, L. Palmisano, M. Schiavello, J. Catal. 134 (1992) 434–444.
[29] Y. Wang, C. Feng, M. Zhang, J. Yang, Z. Zhang, Appl. Catal. B 104 (2011) 268–274.
[30] H. Kato, A. Kudo, J. Phys. Chem. B 106 (2002) 5029–5034.
[31] C.-C. Pan, J.S.C. Wu, Mater. Chem. Phys. 100 (2006) 102–107.
[32] Y. Cong, J. Zhang, F. Chen, M. Anpo, D. He, J. Phys. Chem. C 111 (2007) 10618–10623.
[33] Q. Chen, D. Jiang, W. Shi, D. Wu, Y. Xu, Appl. Surf. Sci. 255 (2009) 7918–7924.
[34] J.G. Yu, H.G. Yu, B. Cheng, X.J. Zhao, J.C. Yu, W.K. Ho, J. Phys. Chem. B 107 (2003) 13871–13879.
[35] I.M. Arabatzis, T. Stergiopoulos, D. Andreeva, S. Kitova, S.G. Neophytides, P. Falaras, J. Catal. 220 (2003) 127–135.
[36] Y.R. Smith, A. Kar, V. Subramanian, Ind. Eng. Chem. Res. 48 (2009) 10268–10276.
[37] I.M. Arabatzis, T. Stergiopoulos, M.C. Bernard, D. Labou, S.G. Neophytides, P. Falaras, Appl. Catal. B 42 (2003) 187–201.
[38] L.A. Galeano, A. Gil, M.A. Vicente, Appl. Catal. B 104 (2011) 252–260.
[39] G.T. Brown, J.R. Darwent, J. Phys. Chem. 88 (1984) 4955–4959.
[40] G. Riegel, J.R. Bolton, J. Phys. Chem. 99 (1995) 4215–4224.